


In vivo investigation of open-pored magnesium scaffolds LAE442 with different coatings in an open wedge defect

Journal of Applied Biomaterials & Functional Materials
1–19
© The Author(s) 2022
Article reuse guidelines:
sagepub.com/journals-permissions
DOI: 10.1177/22808000221142679
journals.sagepub.com/home/jbf


Marlene Schmidt¹ , Anja-Christina Waselau¹, Franziska Feichtner¹ , Stefan Julmi², Christian Klose², Hans Jürgen Maier², Peter Wriggers³ and Andrea Meyer-Lindenberg¹

Abstract

The magnesium alloy LAE442 showed promising results as a bone substitute in numerous studies in non-weight bearing bone defects. This study aimed to investigate the in vivo behavior of wedge-shaped open-pored LAE442 scaffolds modified with two different coatings (magnesium fluoride (MgF₂, group 1)) or magnesium fluoride/calcium phosphate (MgF₂/CaP, group 2)) in a partial weight-bearing rabbit tibia defect model. The implantation of the scaffolds was performed as an open wedge corrective osteotomy in the tibia of 40 rabbits and followed for observation periods of 6, 12, 24, and 36 weeks. Radiological and microcomputed tomographic examinations were performed in vivo. X-ray microscopic, histological, histomorphometric, and SEM/EDS analyses were performed at the end of each time period. μ CT measurements and X-ray microscopy showed a slight decrease in volume and density of the scaffolds of both coatings. Histologically, endosteal and periosteal callus formation with good bridging and stabilization of the osteotomy gap and ingrowth of bone into the scaffold was seen. The MgF₂ coating favored better bridging of the osteotomy gap and more bone-scaffold contacts, especially at later examination time points. Overall, the scaffolds of both coatings met the requirement to withstand the loads after an open wedge corrective osteotomy of the proximal rabbit tibia. However, in addition to the inhomogeneous degradation behavior of individual scaffolds, an accumulation of gas appeared, so the scaffold material should be revised again regarding size dimension and composition.

Keywords

Magnesium alloy, porous scaffold, biodegradation, coating, osseointegration

Date received: 22 July 2022; revised: 1 November 2022; accepted: 9 November 2022

Introduction

Autografts are considered the gold standard for the treatment of bone defects due to their good biocompatibility.^{1,2} However, associated problems include limited availability of donor bone, morbidity at the donor site, and possible inadequate integration into the bone defect with subsequent prolonged hospitalization of patients.^{2–6}

Other bone substitutes such as ceramics in the form of hydroxyapatite and tricalcium phosphate, as well as polymers, showed insufficient stability or biocompatibility in the treatment of large bone defects.^{7–11} For degradable

¹Clinic of Small Animal Surgery and Reproduction, Ludwig-Maximilians-University Munich, Munich, Germany

²Institut für Werkstoffkunde (Materials Science), Leibniz Universität Hannover, Garbsen, Germany

³Institute of Continuum Mechanics, Leibniz Universität Hannover, Garbsen, Germany

Corresponding author:

Andrea Meyer-Lindenberg, Clinic for Small Animal Surgery and Reproduction, Ludwig-Maximilians-Universität, Veterinärstraße 13, Munich 80539, Germany.
Email: ameylin@lmu.de



orthopedic implants, attention was focused on magnesium and its alloys, which showed promising results as solid implants.^{12–17} For instance, screws made of magnesium alloys are used in hallux valgus operations in human medicine.¹⁸ In initial studies, various Mg alloys were also investigated as bone replacement material in the form of open-pored cylinders with promising results in the rabbit model.^{19–23} Several studies have demonstrated that the magnesium ions released during degradation have the advantage of osteogenic and bactericidal effects.^{24–28}

The disadvantage of using Mg-based implants and bone substitutes is the formation of hydrogen gas during the degradation process depending on the alloying components.^{29–31} Controlling the rate of degradation is challenging.²⁹ To decrease the degradation rate of Mg-implants and thereby reduce hydrogen production, different Mg-alloys have been developed and investigated in animal experiments.^{30,32–34} The magnesium alloy LAE442 (4 wt.% lithium, 4 wt.% aluminum, 2 wt.% rare earths) was found to be promising and was intensively investigated as a solid body.^{30,34,35} Porous cylinders of this alloy have also been investigated as bone substitutes in non-weight bearing cancellous bone defects and showed good biocompatibility with slow homogeneous degradation and promising osseointegration.^{21–23}

To further increase corrosion resistance, both Mg solids and bone substitutes are additionally coated.^{36–38} MgF₂ has been reported in the literature to improve corrosion properties and has shown to be very biocompatible.^{21,22,27,39,40} The use of an additional calcium phosphate (CaP) coating on the MgF₂ layer even provided additional corrosion protection.^{19,37,41} It is further described that CaP improves the activity of osteoblasts and promotes bone growth.^{23,42,43} A CaP coating exhibits a similar chemical component to the mineral portion of mammalian bone and is characterized by excellent biocompatibility.^{44–46}

As the accessible literature currently lacks in vivo studies of porous LAE442 scaffolds as a bone graft substitute in partial weight-bearing bone defects, this topic was investigated in the present study. Previous in vitro studies have shown sufficient strength of the alloy for this application.^{37,47} In relation to this, specially designed wedges were investigated in the context of an open-wedge corrective osteotomy in the rabbit tibia.

Material and methods

Scaffold

A number of 40 wedge-shaped scaffolds (height = 10 mm, width = 14 mm, depth = 4.8 mm, Figure 1) were fabricated from the magnesium alloy LAE442 (4 wt.% lithium, 4 wt.% aluminum, 2 wt.% rare earths) by investment casting with an interconnecting pore size of 500 μm.³⁷ All scaffolds were coated with a magnesium fluoride coating (MgF₂) using the “conversion coating” method.³⁷ Half the

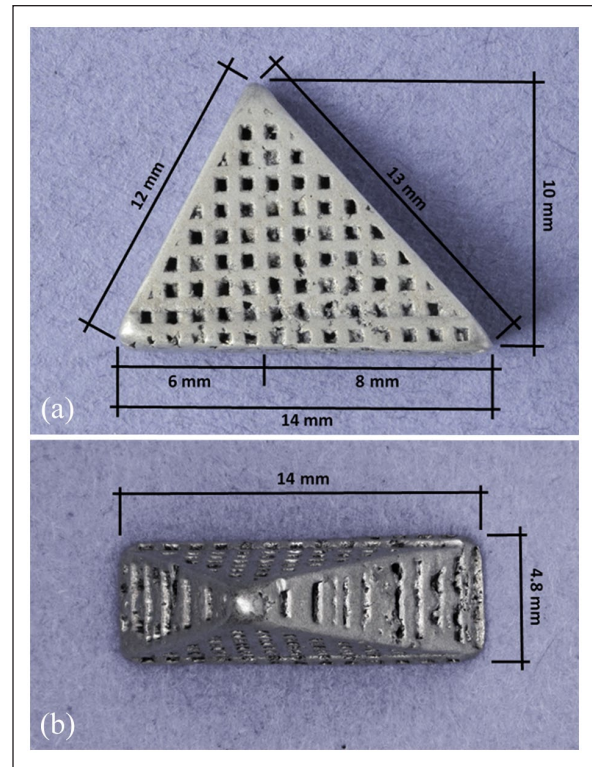


Figure 1. View of the open-pored scaffold (LAE442, CaP coated) with corresponding dimensions: (a) proximal view and (b) lateral view.

scaffolds received no further coating (group 1, $n=20$) and the other half of the scaffolds received a calcium phosphate coating directly onto the MgF₂ coating (CaP, group 2, $n=20$). The scaffolds were immersed into two solutions (first solution: phosphatic solution containing sodium dihydrogen phosphate dehydrate, pH 7.4; second solution: calcium nitrate tetrahydrate) in various circles. The coatings were produced according to the detailed description by Julmi et al.³⁷ With these manufacturing parameters, a reproducible layer thicknesses of approx. 1–2 μm is achieved on the surface of Mg implants, which has been shown, for example, in earlier work by Seitz et al.⁴⁸ As a conversion layer, the layer is largely homogeneous on the surface, but due to the chemical conversion process from Mg(OH)₂ to MgF₂ and especially due to the relatively high roughness of the cast implant surface, local variations of the layer thickness occur. The scaffolds were sterilized with gamma rays (>25 kGy, BBF Sterilisationservice GmbH, Kernen, Germany) before implantation.¹⁹

Animal model

The animal experiment (approval number: ROB 55.2-2532.vet_02-18-125) was approved by the Government of Upper Bavaria according to paragraph 8 of the Animal Protection Act. A total of 40 female adult Zimmermann rabbits (ZiKa Rabbit, Asamhof Kissing, Germany) with a

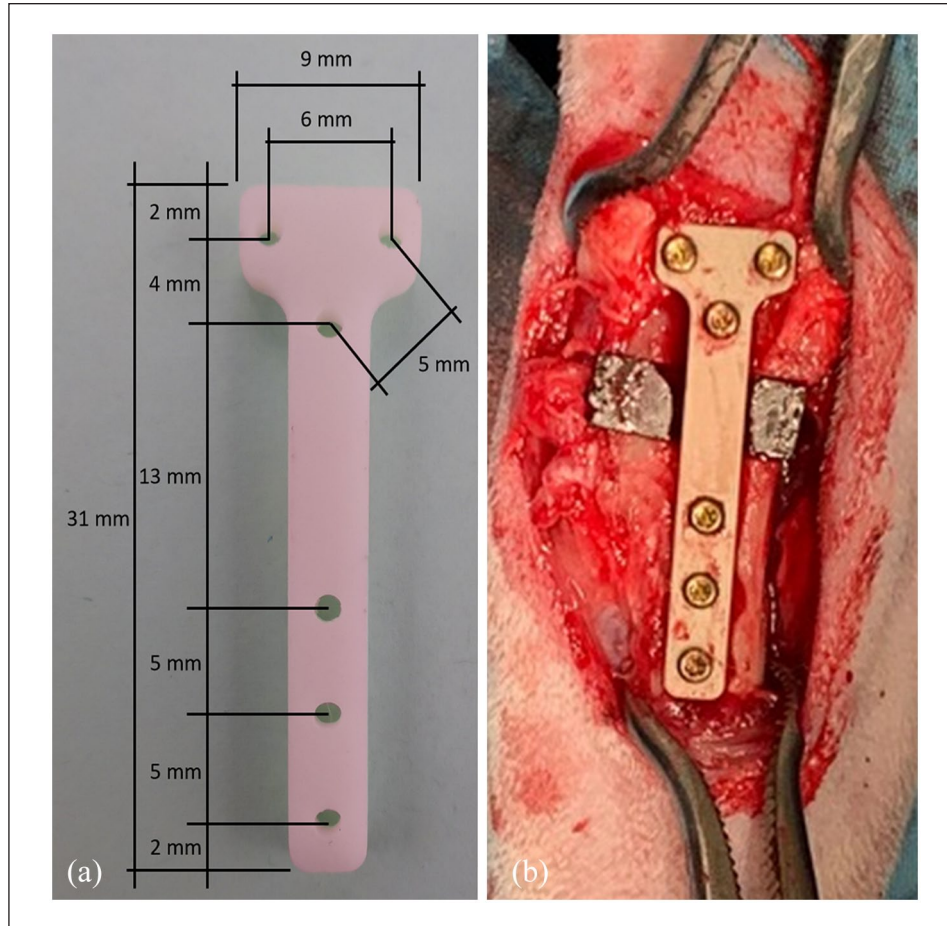


Figure 2. T-plate (PEEK (polyetheretherketone)): (a) with corresponding dimensions and (b) intraoperative view on the tibia with inserted scaffold, plate, and screws.

weight of 4.43 kg (± 0.29 kg) were used. The animals were randomly assigned to four time groups (6, 12, 24, and 36 weeks). Six animals were used in each group. To reduce the number of animals and to obtain an intermediate trend after 24 weeks, two animals per coating group were additionally implanted and evaluated for this time point.

Surgery and euthanasia

Preoperatively, the animals received enrofloxacin (10 mg/kg, Enrobactin[®], CP-Pharma GmbH, Burgdorf, Germany) as an antibiotic and meloxicam (0.3 mg/kg, Meloxicam, Rheumocam[®], Albrecht GmbH, Aulendorf, Germany) orally as pain prophylaxis. For induction of anesthesia, ketamine (15 mg/kg, Anesketin[®] 100 mg/ml, Albrecht GmbH, Aulendorf, Germany) and medetomidine (0.25 mg/kg, Dorbene vet[®] 1 mg/ml, Zoetis Deutschland GmbH, Berlin, Germany) were administered intramuscularly. Anesthesia was maintained after intubation with an isoflurane/oxygen mixture. The surgical field was circularly shorn from the greater trochanter ossis femoris to the distal tibia and aseptically prepared. Intraoperative analgesia was provided with

fentanyl infusion (3 μ g/kg, Fentadon[®], 50 μ g/ml, CP-Pharma Handelsgesellschaft GmbH, Burgdorf, Germany).²² The rabbits were placed in the lateral position on the operating table and the right leg was sterily draped and positioned in slight flexion to allow medial access to the proximal tibia. An approximate 4 cm skin incision was made, and the transection of subcutaneous tissue and deep fascia was followed by exposure of the medial collateral ligament. Cranial and caudal muscles were held aside using Hohmann levers. Using an oscillating saw under sterile water cooling (Colibri II, DePuy Synthes[®], Synthes GmbH, Oberdorf, Switzerland), a wedge-shaped piece of bone corresponding to the size of the scaffold was sawn out distally of the medial collateral ligament with the aid of a template while preserving the fibula. While stabilizing the bone defect with reduction forceps, the scaffold was inserted with a precise fit. To hold the wedge in position and to support the tibia, it was then fixed with a custom-made T-plate (Figure 2(a)) made of non-absorbable plastic (9 mm \times 31 mm, PEEK (polyetheretherketone), RISystem AG, Landquart, Switzerland) and six titanium screws (three proximal, three distal) (Cortex Screw Stardrive \varnothing 1.5 mm, DePuy Synthes[®], Synthes GmbH, Oberdorf,

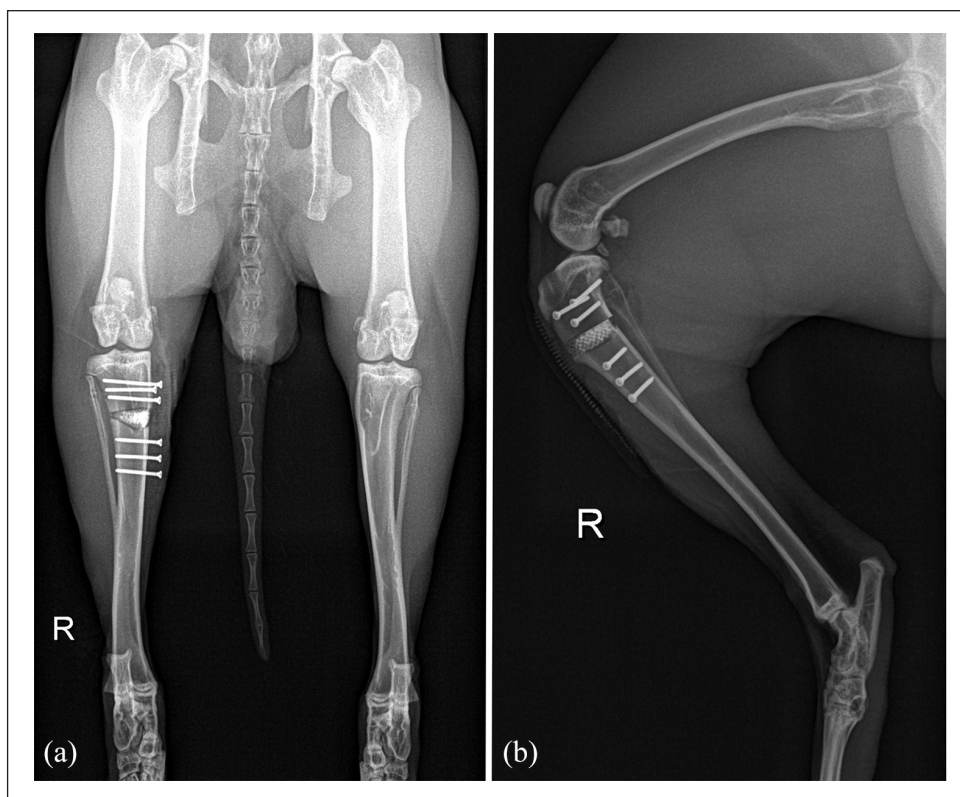


Figure 3. X-ray images in (a) craniocaudal and (b) mediolateral view post-op (the plate is generally not visible in radiodiagnostic images).

Switzerland) (Figure 2(b)). The fascia was then adapted with single staples and a continuous subcutaneous suture (Monosyn violet 4/0, B. Braun Melsungen AG, Melsungen, Germany). The skin was closed with single staples (Optilene blue 4/0, B. Braun Melsungen AG, Melsungen, Germany). Postoperative μ CT and X-ray images were taken to check the correct fit of the scaffold. As postoperative pain therapy, buprenorphine (20 μ g/kg, intravenously directly postoperatively, otherwise subcutaneously) (Bupresol[®], 0.3 mg/ml, CP-Pharma Handelsgesellschaft GmbH, Burgdorf, Germany) was given three times daily for 4 days and meloxicam daily until the fifth postoperative day. The animals were given daily antibiotic prophylaxis with enrofloxacin until the fifth postoperative day. Thereafter, the animals received metamizole (Novaminsulfon – 1A Pharma[®], 20 mg/kg, 1A Pharma GmbH, Oberhaching, Germany) and meloxicam two to three times daily if required. The animals wore a cervical collar for 10 days and received Bene-Bac (Bene-Bac[®] Gel, 0.5 g/animal/day, Dechra Veterinary Products Deutschland GmbH, Aulendorf, Germany) to support the digestive system during this time. Clinical and orthopedic evaluations of the animals were performed daily for 14 days post-op and at regular intervals thereafter. At the end of the observation period, the animals were euthanized painlessly using pentobarbital (Narkodorm[®] 200–800 mg/kg, CP-Pharma, Burgdorf, Germany). After harvesting the tibia including the fibula

and removing the soft tissue, the bone-implant samples were extracted using a diamond band saw (cut-grinder, Messner GmbH, Oststeinbek, Germany). The samples were cut proximal and distal to the adjacent screws. Samples were fixed in a 4% formalin solution for at least 5 days.

Radiological examination and evaluation

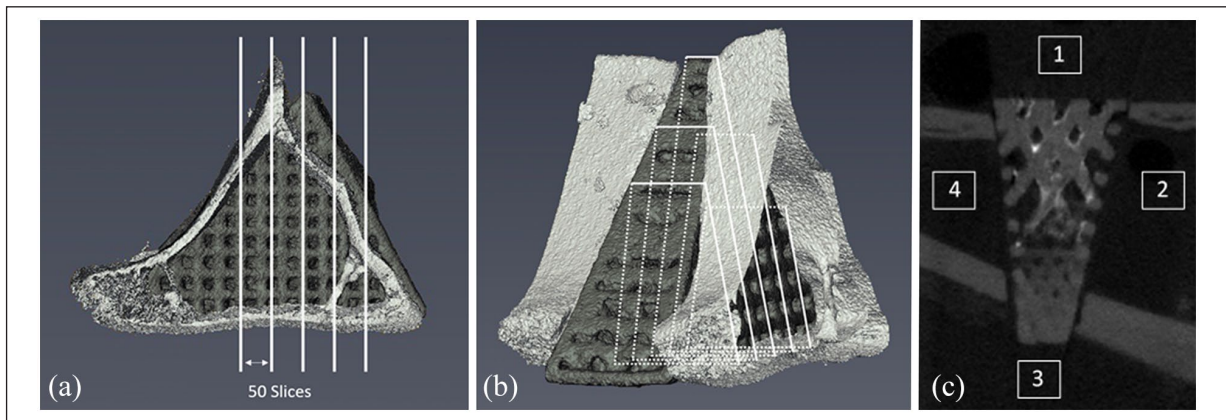
Radiographs of the hindlimbs (Multix Select DR, Siemens Healthcare GmbH, Erlangen, Germany) in craniocaudal (krkd) and mediolateral (ml) view were taken at 2-week intervals until week 12 and every 4 weeks thereafter (Figure 3) with the setting of 54.9 kV and 4.5 mAs. The evaluation was done using dicom-PACS[®] software (version 8.3.20; Oehm und Rehbein GmbH, Rostock, Germany). The parameters for scaffold fit, screw position, scaffold degradation, callus formation at the osteotomy gap, gap between scaffold and bone, and gas inclusions in the vicinity of the scaffold were assessed descriptively.

In vivo μ CT examination and evaluation

In vivo μ CT scans (XtremeCT II, Scanco Medical, Zurich, Switzerland) were obtained under sedation (medetomidine 0.25 mg/kg and ketamine 15 mg/kg) according to the

Table 1. Scoring system for μ CT evaluation. Parameters were scored at each scan timepoint. The lowest value of 0 represents the desired result.

| Scoring parameter | Score 0 | 1 | 2 | 3 | 4 |
|---|---|--|--|--|--|
| Gas in the surrounding tissue | None | Diffuse ($\varnothing < 1$ mm) | Low grade ($\varnothing < 5$ mm) | Medium grade ($\varnothing: 5-10$ mm) | High grade ($\varnothing < 10$ mm) |
| Gas in the medullary cavity | None | Diffuse ($\varnothing < 1$ mm) | Low grade ($\varnothing < 2.5$ mm) | Medium grade ($\varnothing < 5$ mm) | High grade ($\varnothing > 5$ mm) |
| Osteotomy gap closed from the outside (covered with callus) | Complete bridging (100%) | >75% callus | >50% callus | >25% callus | No or minimal bridging via callus tissue |
| Scaffold integration (reoriented scan) | 100% contact surface between bone and scaffold, no gaps | >75% contact area between bone and scaffold, only minimal gaps | >50% contact area between bone and scaffold, isolated gaps | >25% contact area between bone and scaffold, larger gaps | No or slight contact between bone and scaffold, clear gaps |

**Figure 4.** (a and b) Illustration of the five standardized cross-sections of the scaffold in the reoriented scan and (c) central reoriented cross sections with directional positions: (1) medial, (2) proximal, (3) lateral, and (4) distal.

radiological examination interval. The scan area included the proximal tibia including the scaffold and the implant. The following settings were chosen: tube voltage 68 kV, current 1470 μ A, 1000 projections/180°, integration time 250 ms, and isotropic voxel size 30.3 μ m. The images were evaluated descriptively, semiquantitatively and quantitatively by two observers using the μ CT Evaluation Program V6.6 software (Scanco Medical, Zurich, Switzerland).

Descriptive and semiquantitative evaluation of the μ CT examination. Scaffold shape and scaffold degradation were descriptively evaluated in the original scan (transverse plane). The semiquantitative evaluation was performed by two observers using a scoring system (Table 1). Gas accumulation in surrounding tissues or in the medullary canal (which were measured with the ruler option of the evaluation software) and bridging of the osteotomy gap with callus were evaluated in the transverse plane. The scaffold scans were reoriented to evaluate scaffold integration (bone-scaffold contacts) using five standardized scaffold cross-sections in the sagittal plane (Table 1, Figure 4).

Quantitative evaluation of the μ CT examination. Scaffold degradation was analyzed quantitatively at each scan time point by calculating the volume and density of the scaffolds. A threshold of 146 was used for LAE442 according to the literature.²¹⁻²³

X-ray microscopy images

The scaffolds were scanned before implantation and after explantation using an X-ray microscope (Zeiss Xradia 410 Versa, Carl Zeiss Microscopy GmbH, Jena, Germany). Pre-implantation scans were obtained with a pixel size of 10 μ m, a voltage of 60 kV, and an exposure time of 1.5 s. Explanted scaffold bone composites were scanned with a pixel size of 6 μ m, a voltage of 50 kV, and an exposure time of 2 s. The scans were generated using a flat panel and a power of 4 W. Using these high-resolution X-ray microscope scans, the volumes of all scaffolds were analyzed before implantation and at the end of each study period and compared with the data from μ CT. Volumes were calculated with the μ CT evaluation program V6.6 software (Scanco Medical, Zurich, Switzerland) by using a

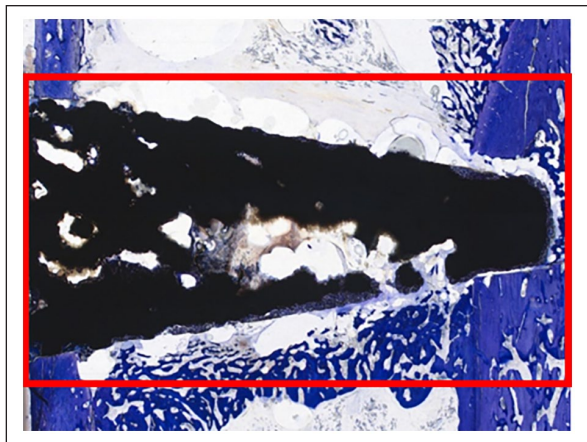


Figure 5. Central histological cross-section containing the measurement frame (2600 pixels \times 1450 pixels) for histomorphometric evaluation.

scan-specific threshold according to the half maximum height (HMH) protocol.⁴⁹

Histological examination and evaluation

After the formalin-fixated samples were scanned using the X-ray microscope, they were dehydrated in an ascending series of alcohol, defatted with xylene (Carl Roth GmbH, Karlsruhe, Germany) and embedded in Technovit 9100 (Technovit® 9100, Heraeus Kulzer GmbH, Wehrheim, Germany). 80 μ m histological sections as a longitudinal sections were produced using the cutting and grinding technique according to Donath and Breuner.⁵⁰ The sections were made using longitudinal cuts in the center of the plate in a mediolateral direction (Figure 5) with a diamond band saw and then ground down to the appropriate thickness (cut grinder and lap grinder, Messner GmbH, Oststeinbek, Germany). Histological sections were surface stained with 0.1% toluidine blue O (Waldeck, Münster, Germany). Two central sections from the wedge center with adjacent cortical bone and plate were evaluated descriptively, semiquantitatively and quantitatively using an optical microscope (Axio Imager.Z2, Carl Zeiss Microscopy GmbH, Jena, Germany).

Descriptive and semiquantitative histological evaluation. In two sections per specimen, remodeling of the cortices, the amount of callus and gas bubbles (which were measured with the ruler option of the evaluation software), degradation of the scaffold and the bridging of the osteotomy gap were assessed using a semiquantitative scoring system by two observers at 2.5 \times magnification (Table 2). The presence of cartilaginous tissue, macrophages, foreign body giant cells, adipocytes, blood vessels, and newly formed tissue at the scaffold edge or in the pores, as well as changes in the scaffold, such as cracks, were descriptively assessed at 20 \times magnification.

Quantitative histological evaluation. As with the semiquantitative evaluation, two central sections of each sample were evaluated histomorphometrically. The sections were photographed as micrographs with a 2.5 \times magnification using the Zeiss Axiocam microscope camera (Carl Zeiss Microscopy GmbH, Jena, Germany) and the Zeiss ZEN2 software (Carl Zeiss Microscopy GmbH, Jena, Germany) and analyzed histomorphometrically using Zen Intellesis software. For automated segmentation, an AI (artificial intelligence) model based on machine learning was trained. All sections were segmented and evaluated identically. For this purpose, a measurement frame of 2600 pixels \times 1450 pixels was placed over the scaffold and adjacent structures (Figure 5). When placing the measuring frame, care was taken to include as few parts of the fixation plate as possible.

The percentage area of the following elements was calculated: scaffold, bone, gas, granulation tissue, osteoid, plate, bone marrow, and cartilage.

SEM/EDS analyses

Scanning electron microscope (SEM) images were taken of unstained histological sections prepared as described in 2.7 according to Maier et al.³⁶ to characterize the surfaces of the scaffolds. Energy-dispersive X-ray spectroscopy (EDS) analyses were performed in selected areas to determine the composition of the elements. Images of the histological sections were recorded by SEM (SUPRA 55 VP; Carl Zeiss AG, Oberkochen, Germany) with X-ray spectroscopy (EDX) analysis at an acceleration voltage of 15 kV. One section of an intact scaffold was measured for each time and coating group. Furthermore, one section of a severely degraded scaffold per coating group of weeks 12, 24, and 36 was measured to identify the cause of the severe degradation. Measurements were taken in the scaffold center, in the degradation layer, in bone and within conspicuous bright areas of the scaffold.

Statistics

Statistical analyses were performed using “Microsoft Excel 2016” (Microsoft Corporation, Redmond, WA 98052–6399, USA) and “SPSS Statistics 26.0” (IBM, Armonk, NY 10540, USA). This analysis was based on the comparison of the two groups in relation to the study interval. The semiquantitative μ CT- and histology data were analyzed using the Mann-Whitney U test. Quantitative data (μ CT, histomorphometry, and X-ray microscopy) were tested for normal distribution using the Shapiro-Wilk test. For normally distributed data, Levene’s test was performed followed by Welch’s or Student’s t -test. For non-normally distributed data, the Mann-Whitney U test was used. In all tests, a value of $p < 0.01$ was considered statistically significant.

Table 2. Scoring system for histological evaluation. The parameters were scored using two cross-sections per scaffold. The lowest value of 0 represents the desired result.

| Scoring parameter | Score 0 | 1 | 2 | 3 | 4 |
|---|---|--|--|--|--|
| Gas in the surrounding tissue | None | Diffuse ($\varnothing < 1$ mm) | Low grade ($\varnothing < 5$ mm) | Medium grade ($\varnothing: 5\text{--}10$ mm) | High grade ($\varnothing < 10$ mm) |
| Gas in the medullary cavity | None | Diffuse ($\varnothing < 1$ mm) | Low grade ($\varnothing < 2.5$ mm) | Medium grade ($\varnothing < 5$ mm) | High grade ($\varnothing > 5$ mm) |
| Osteotomy gap closed from the outside (covered with callus) | Complete bridging (100%) | >75% callus | >50% callus | >25% callus | No or minimal bridging via callus tissue |
| Scaffold integration (reoriented scan) | 100% contact surface between bone and scaffold, no gaps | >75% contact area between bone and scaffold, only minimal gaps | >50% contact area between bone and scaffold, isolated gaps | >25% contact area between bone and scaffold, larger gaps | No or slight contact between bone and scaffold, clear gaps |

Table 3. Scaffolds with loss of shape, presented with corresponding time points for the different evaluation methods.

| Group (material) | Macroscopic onset of severe degradation (in vivo μ CT) | Time group, severe degradation in ex vivo analyses (X-ray micrographs and histology) |
|------------------|--|--|
| 1 | Week 4 | 12 |
| 1 | Week 4 | 12 |
| 1 | Week 6 | 12 |
| 1 | Week 12 | 24 |
| 1 | Week 16 | 36 |
| 1 | Week 24 | 36 |
| 1 | Week 24 | 36 |
| 2 | Week 4 | 12 |
| 2 | Week 4 | 12 |
| 2 | Week 8 | 12 |
| 2 | Week 8 | 12 |
| 2 | Week 8 | 12 |
| 2 | Week 12 | 24 |
| 2 | Week 6 | 36 |

Results

Clinical examination

All animals recovered well from surgery and wound healing was uneventful. Most of the animals in both groups (23/40) showed mild to moderate lameness and little evidence of pain up to a maximum of 16 days post-surgery. Only one animal in group 2 showed persistent low-grade lameness after surgery until the end of the observation period in week 12. Palpatory emphysematous swelling medial to the proximal tibia was found in 36/40 animals from postoperative day 10 until a maximum of 6 weeks post-surgery. In 14 animals, a puncturing of the swelling was indicated once due to marked lameness (grade 3) with weight loss and pain on palpation. Gas (<2 ml) mixed with fluid (2–5 ml (seroma)) was withdrawn from the swelling and the lameness disappeared. Bacteriological testing of

the fluid was inconclusive in both aerobic and anaerobic cultivation. The histological smear of the fluid was relatively lacking in cells, with only isolated blood cells found.

Radiological evaluation

Postoperative radiographs demonstrated the correct positioning of the scaffolds and screws. In one animal (with the existing lameness) the screw proximal to the osteotomy gap was not anchored in the contralateral cortex and bent. Initial scaffold degradation was observed in group 2 in week 4 and in group 1 in week 20. All scaffolds remained clearly visible throughout the study period. Callus formation was seen in both groups starting in week 4. In week 28 (group 1) and week 32 (group 2), the osteotomy gap was completely bridged with callus from all sides in all animals (Supplemental Material 1(a) and (b)). Gap formation in the area between the scaffold and the proximal or distal bone (MgF_2 : 8/20; CaP: 9/20), was visible in both planes from the second postoperative week until week 10 (group 1) or week 16 (group 2) (Supplemental Material 1(c) and (d)). Significant gas accumulation occurred in the surrounding tissue of the proximal tibia from week 2 to week 16 (group 2) and week 24 (group 1) in the majority of animals (group 1: 19/20; group 2: 17/20) (Supplemental Material 1(c) and (d)).

In vivo μ CT examination and evaluation

Descriptive and semiquantitative evaluation of the μ CT examination. The majority of the scaffolds (26/40) kept most of their original contour until the end of the respective study period. No macroscopic degradation was visible. The other scaffolds (14/40) (per group: $n=7$) showed structural loss with severe degradation (Table 3, Figure 6). In these 14 scaffolds, initial degradation was observed in week 4. In group 1, it started mostly at the scaffold tip and spread homogeneously over the entire scaffold during the

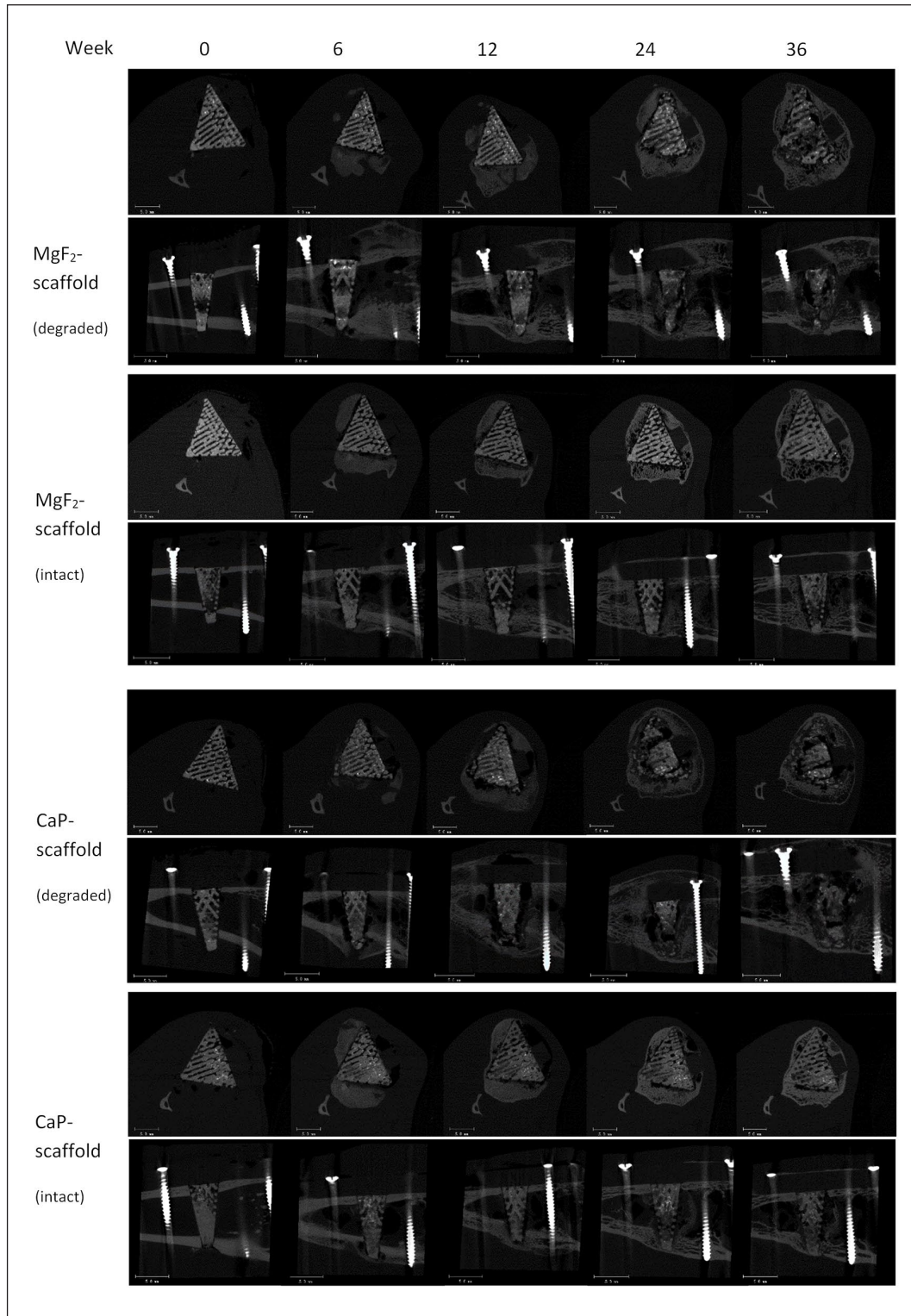


Figure 6. μ CT images of the center of intact and severely degraded scaffolds in the original and the reoriented scan.

course of the study. In group 2, the majority of this increased degradation was homogeneous. Gas formation was observed outside the bone and intramedullary in the proximal tibia. Gas outside the bone was detected until

week 32 with steadily decreasing amounts in the surrounding soft tissue (Figure 7(a)). There was an increase in the amount of intramedullary gas at weeks 2 and 4 for both groups, followed by a decrease until week 16 (group

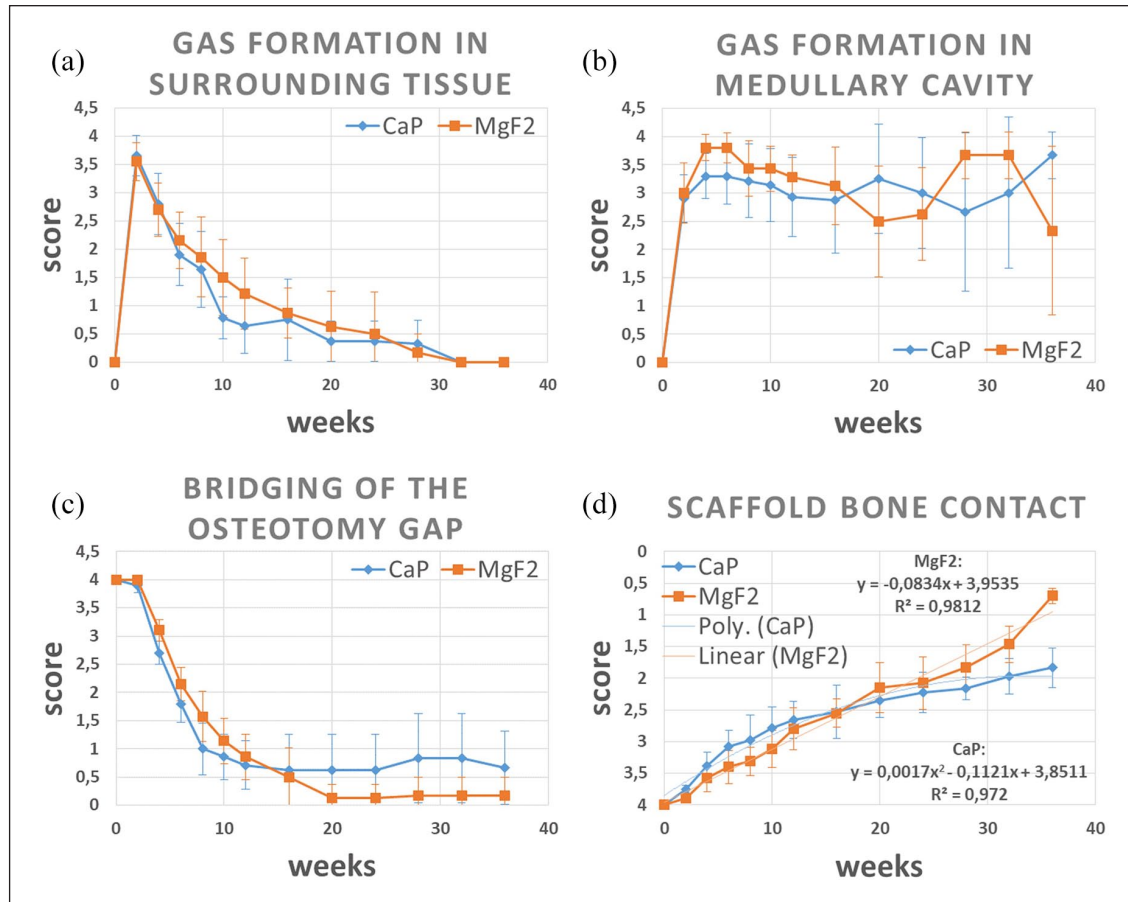


Figure 7. Semiquantitative analysis of the μ CT scans: (a) gas formation in the surrounding tissue, (b) gas formation in the medullary cavity, (c) bridging of the osteotomy gap, and (d) bone scaffold contact.

2) and 20 (group 1), respectively. Thereafter, the intramedullary gas formation differed in both groups (Figure 7(b)). Initial callus formation was observed in week 2 (group 2) or week 4 (group 1) in the scaffold tip area (transcortex, lateral cortex). After week 6, the osteotomy gap was >50% bridged with callus tissue (Figure 7(c)). At weeks 12 and 16, callus tissue appeared to be inhomogeneous in all scaffolds. Starting in week 20, bone maturation with lamellar bone was evident in group 1 and in week 24 in group 2. In week 36, the last observation time point, the osteotomy gap was completely bridged with the exception of a few scaffolds (group 1: $n=1$; group 2: $n=3$). Postoperatively, the optimal positioning and the contact of the scaffolds with the cortices could be demonstrated in the reoriented μ CT scans in 36/40 scaffolds. In 4/40 CaP-scaffolds, a small gap between scaffold and laterodistal and mediolateral cortex was observed. By postoperative week 2, all scaffolds showed developing bone-scaffold contacts (Figure 7(d)), with newly formed bone tissue uniformly approaching the scaffolds. From week 4 onward, both groups showed more contacts in the caudal region of the scaffold compared with the cranial region. Overall, a higher number of bone-scaffold contacts were

seen from week 2 to week 16 in group 2, and from week 16 to week 36 in group 1.

Quantitative evaluation of the μ CT examination. The scaffolds of both groups showed small volume decreases from the time of implantation to the end of the study at week 36 (Group 1: 8.9%; Group 2: 7.5%) (Figure 8(a)). There was also a decrease in density for both coatings (Group 1: 16.07%; Group 2: 23.65%) (Figure 8(b)).

X-ray microscopic images

The high-resolution X-ray microscope scans demonstrated the integrity of all scaffolds prior to implantation. One scaffold from group 1 showed a lower number of pores in the central area than in the other samples. Differences in the initial volume of the scaffolds were evident (Supplemental Material 2). In the images taken at the respective end of the study, severe degradation and loss of shape of the scaffolds were observed in 14/40 scaffolds (seven per group, Table 3). The volume loss of the scaffolds before implantation and at the end of the study in week 36 was relatively low (group 1: 11.8%; group 2: 5.8%) (Supplemental Material 2).

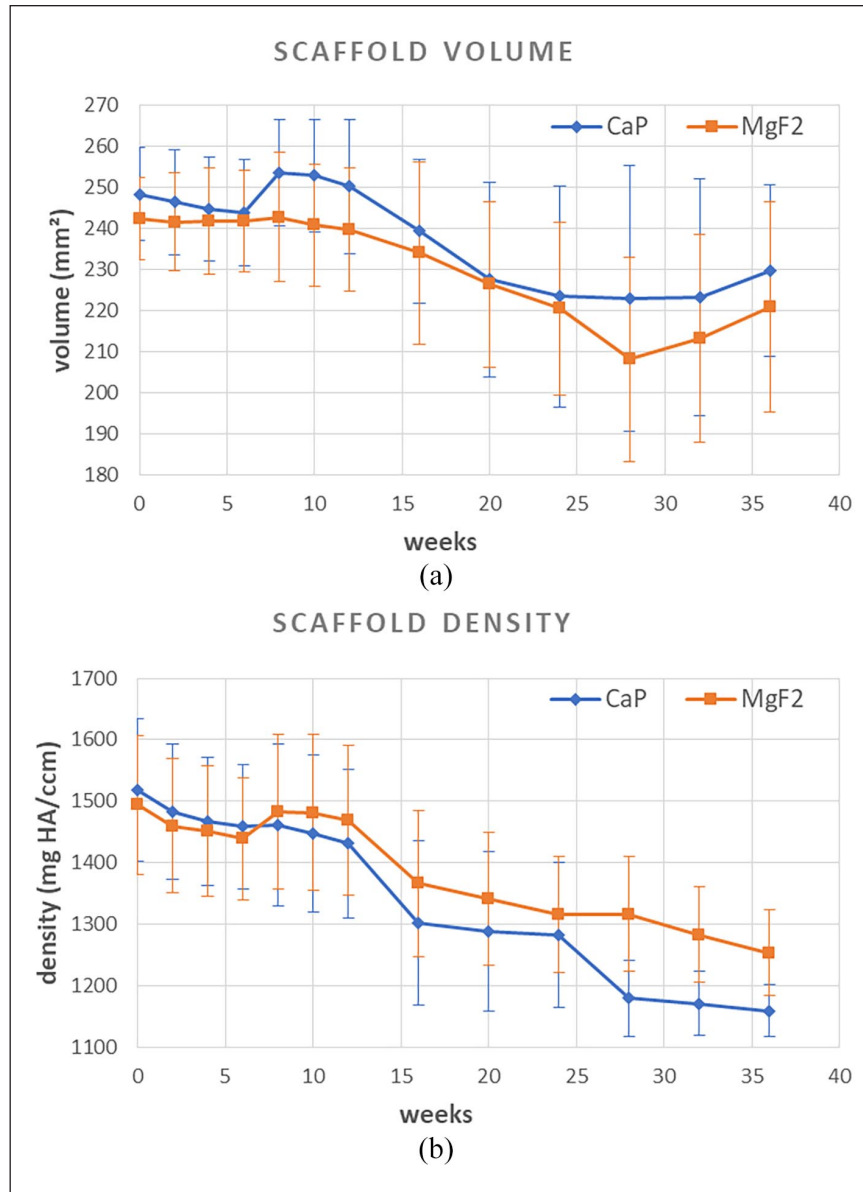


Figure 8. Quantitative evaluation of the μ CT scans: (a) scaffold volume and (b) scaffold density.

Histological evaluation

Descriptive and semiquantitative evaluation. The semiquantitative evaluation for time points 6 and 36 weeks of implantation showed more degradation in group 1 (Figure 9(a)). In week 12, degradation was greater in group 2 and in week 24 it was identical in both groups. Overall, it was noticeable that 14/40 scaffolds (seven each per group, Table 3) degraded more severely or less homogeneous than the rest. This was manifested in the loss of their original shape (Figure 10). Massive periosteal callus was present on the lateral side of the tibia after 6 and 12 weeks in both groups and was seen to a smaller extent at later examination time points after 24 and 36 weeks (Figures 9(b) and 10). In week 6, five CaP scaffolds and three MgF₂ scaffolds showed an incompletely bridged osteotomy

gap at the scaffold tip. Complete bridging was noted at later observation time points (Figure 9(c)). Small amounts of endosteal callus tissue were present in both groups after 6 and 12 weeks which increased over time. Overall, greater amounts of endosteal callus tissue were seen distal to the scaffolds than proximally (Figure 9(d) and (e)). From week 6 onward, both groups showed increasing remodeling of the cortices over time with a greater extent at the trans-cortex (cortex near the tip of the scaffold) (Figure 9(f)–(i)). Gas was observed mainly in the proximal region of the scaffold in the medullary cavity (Figure 9(j) and (k)). Overall, gas formation persisted to a moderate extent throughout the course of the study. At the 6-week time point, cracks were seen in the scaffold tip region. Over time, cracks were observed over the entire scaffold

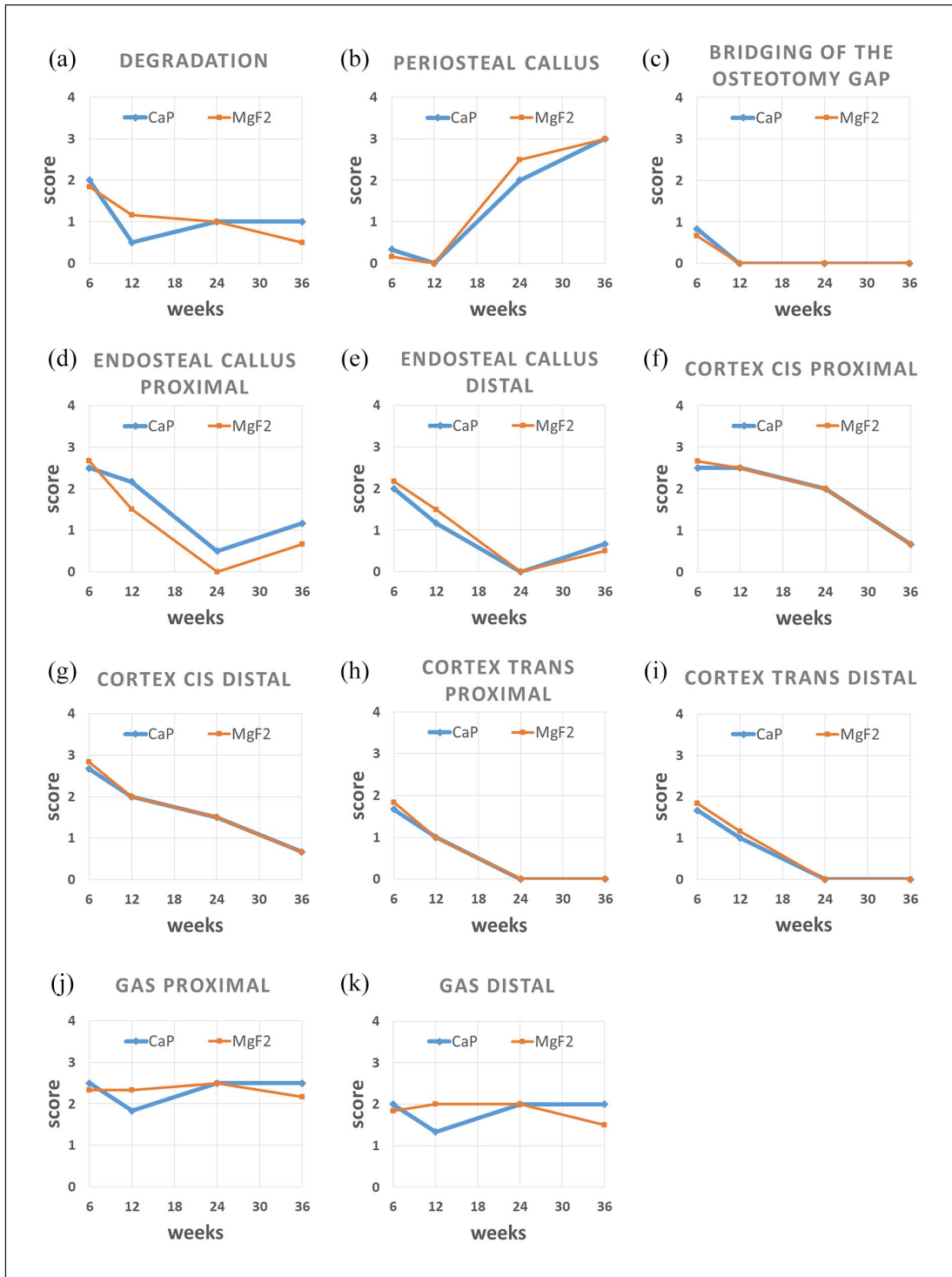


Figure 9. Semiquantitative evaluation of the histological sections : (a) degradation, (b) periosteal callus, (c) bridging of the osteotomy gap, (d) endosteal callus proximal, (e) endosteal callus distal, (f) cortex cis proximal, (g) cortex cis distal, (h) cortex trans proximal, (i) cortex trans distal, (j) gas proximal, (k) gas distal.

surface, with MgF₂ scaffolds showing more cracks than CaP scaffolds. Cartilage tissue was evident in individual scaffolds after week 6 (2× group 1, 4× group 2), week 12 (1× group 1, 1× group 2), and week 24 (1× group 2) in the area of the

lateral osteotomy gap. In week 6, osteoid could be seen at the tip of the scaffolds in both groups. In week 12, thicker osteoid seams were seen in the tip and distal surface of the scaffold which surrounded the entire scaffold after 24 and 36 weeks

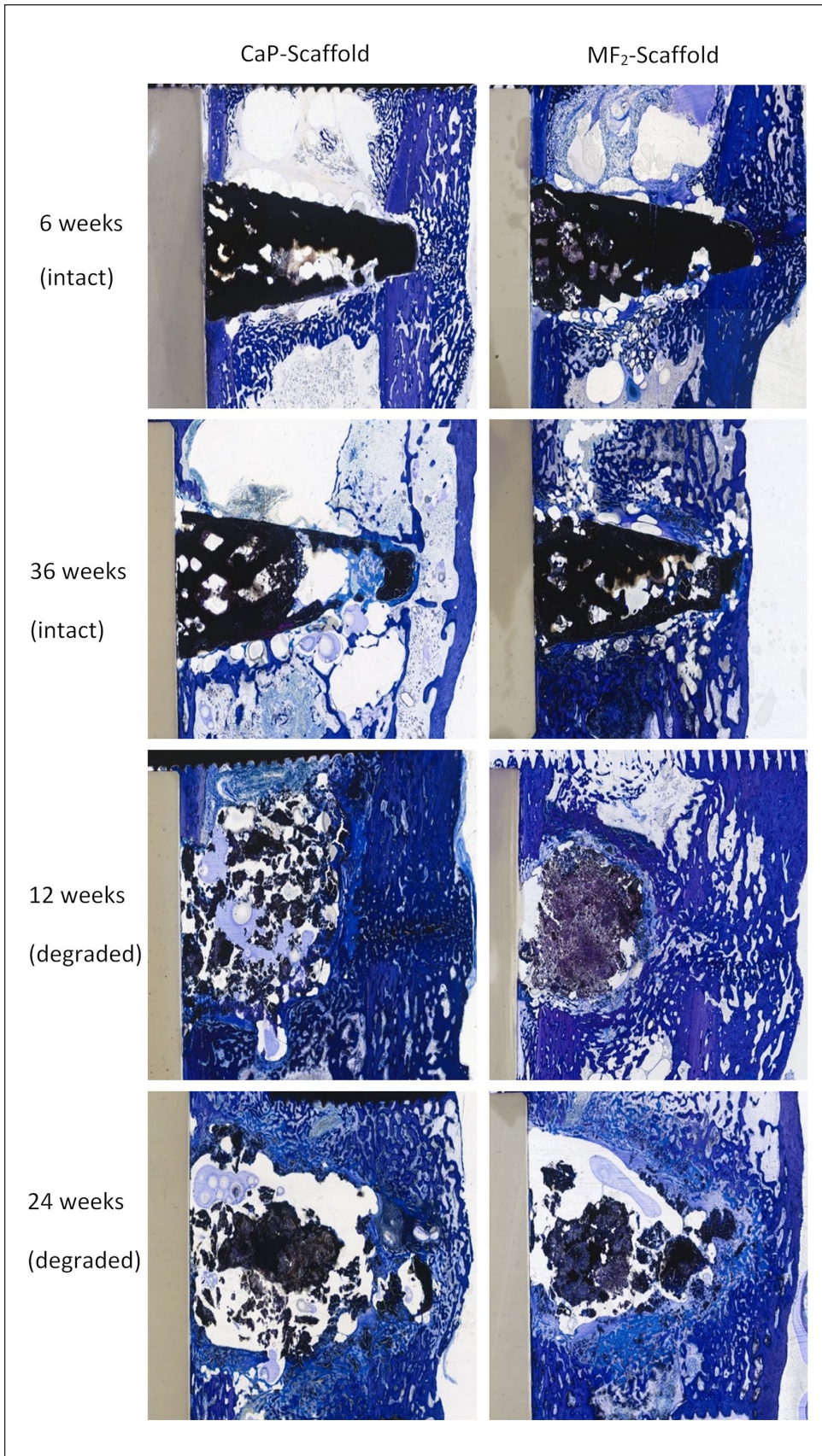


Figure 10. (Continued)

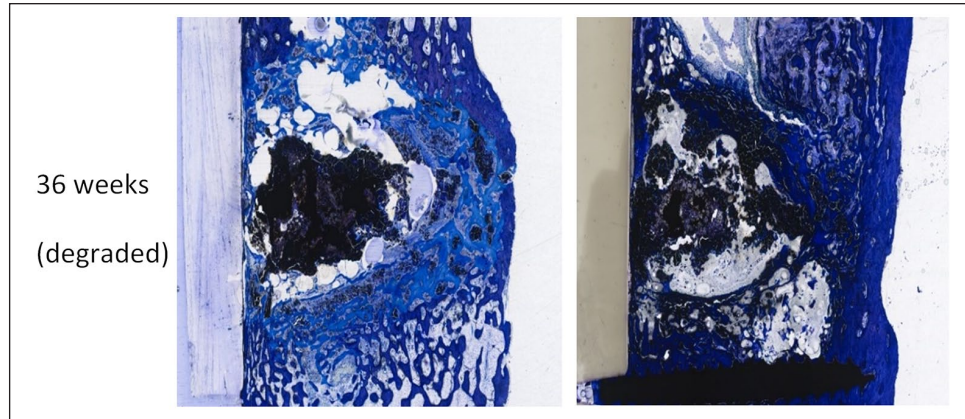


Figure 10. Histological cross-sections of intact scaffolds (upper two rows) and severely degraded scaffolds (lower three rows) of both coatings.

and sporadically extended into outer pores. On the proximal and distal surfaces of the scaffold, excluding the tip, a narrow granulation tissue fringe consisting of fibroblasts and fibrocytes was evident after 6 weeks in both groups which sporadically grew into the outer pores of the scaffolds. At week 12, a slightly more pronounced granulation tissue layer was present around the scaffold and between the callus network. At weeks 24 and 36, granulation tissue was almost exclusively evident between the callus network. In week 36, granulation tissue and osteoid could be seen in individual central pores. Bone tissue was not detected in the pores at any time.

Bone marrow located distal and proximal to the scaffolds increased over time and was characterized by many adipocytes and cells in various stages of the myeloid series. Furthermore, a moderate amount of macrophages and scattered blood vessels were seen in the medullary cavity after 6 weeks which increased over time. In week 36, more blood vessels were seen in group 1 than in group 2. Foreign body giant cells were observed only sporadically in both groups at weeks 24 and 36.

Quantitative histological evaluation. The histomorphometric evaluation (Supplemental Material 3) of both groups showed only a slight loss of material between weeks 6 and 36 (group 1: 7.3%, group 2: 2.5%). The histomorphometrically measured bone quantity (week 6: group 1: 25.3%, group 2: 16.7%) increased overall over time and reached the highest values in week 36 (group 1: 30.7%, group 2: 26.3%). It was noticeable that more bone was measured in all observation times in group 1 than in group 2. Gas was detected at all time points, with the highest gas content detected in both groups in week 24. Comparing the two groups, it was noticeable that significantly less gas was measured in group 1 than in group 2 in weeks 6, 24, and 36 (week 6, $p=0.008$). In contrast, group 1 showed significantly more gas than group 2 in week 12 ($p=0.003$). Regarding the area percentage of granulation tissue, group 1 showed a constant value of about 12% over the study period. In contrast, granulation

tissue in group 2 decreased from an initial 14.7% in week 6 to 5.6% in week 24 and increased again to 8% in week 36. Osteoid was seen at all examination time points. In group 2, the amount of osteoid increased steadily over time (week 6: 0.9%; week 36: 6.0%) and had a significantly greater proportion than group 1 at the 36-week time point ($p=0.0014$). Bone marrow tissue was detected to a similar extent in both groups and remained relatively constant over time (week 6: group 1: 6.3%, group 2: 5.6%). Cartilage tissue was measured to a very low extent in both groups. The amount of plate that could technically not be excluded from the measurements remained in the range below 1%.

SEM/EDS analyses

The SEM images showed a clearly distinguishable degradation layer in all scaffolds which appeared darker compared to the original scaffold material (Supplemental Material 4: measuring point 4; Supplemental Material 5: measuring points 1, 6). The extent of this degradation layer increased over time. Heavily degraded scaffold material showed a lot of bright islands in the SEM images. EDS analyses in this area showed that these bright spots were strong enrichments of rare earths and aluminum (Supplemental Material 5: measuring points 4, 5). Using EDS analyses, magnesium was detected in decreasing amounts from the scaffold center to the periphery with surrounding bone (Supplemental Material 4: measuring points 2, 3, 4). The amount of magnesium decreased as the implantation time progressed (Supplemental Material 4: measuring point 3; Supplemental Material 5: measuring point 3). On the scaffold surface and in the degradation layer, regions with rare earths, aluminum, and also calcium and phosphate (Ca/P) could be identified (Supplemental Material 4: measuring points 1, 5; Supplemental Material 5: measuring point 4, 5). Ca/P precipitates were found in contact points between new bone tissue and the scaffold.

Discussion

The clinically good tolerability of the magnesium alloy LAE442 has been confirmed in other studies.^{17,34,51} In the present study, no clinical adverse reactions and only mild to moderate lameness were observed in 24/40 animals, which may be attributed to the surgical procedure of a hinged corrective osteotomy. Another cause of this lameness could be gas or seroma formation, as lameness improved after a single puncture of the affected site in these animals. It is known that hydrogen is produced during the degradation of magnesium, which accumulates locally if it is insufficiently removed by the surrounding tissues and blood vessels.^{30,52,53} A causal relation between lameness and accumulation of gas due to degradation of magnesium alloys has not been observed in other studies.^{30,52,54,55} Intramedullary gas bubbles, which were observed in the medullary cavity in the vicinity of the scaffolds, remained at a moderate level over the time course of the present study and have been described many times in other studies in connection with intramedullary pins and an interlocking nail system made of LAE442 in animal models.^{16,56,57} The occurring seromas probably originated from the irritation of the skin with the underlying tissue and a surgical-induced wound cavity.^{20,58,59} The existing lameness of one animal can be attributed to the obliquely placed screw.

The gas accumulation seen immediately postoperatively is air that was physiologically entrapped intraoperatively and is unrelated to the degradation of the scaffolds.^{19–22}

The different initial volume of the scaffolds found in the X-ray microscope investigations can be attributed to the manufacturing process. The production of the wedges of this size, dimension, and standardized pore sizes proved to be very difficult in the investment casting process.³⁷ Quantitative analyses of volume and density using μ CT, X-ray microscopy, and histomorphometry showed a very slow degradation of the scaffolds with small volume and density decrease until the end of the study at week 36. The slow degradation of the magnesium alloy LAE442 was also observed on small-sized porous LAE442 cylinders which were investigated in the greater trochanter of the femur in the rabbit model.^{21–23,60,61} When comparing the coatings in the present study, it was noticed that the wedges coated only with MgF_2 (group 1) showed an overall greater volume loss than the wedges additionally coated with CaP (group 2). This indicates that additional coatings slow down degradation and at the same time gas formation. In a previous study by Julmi et al.,³⁷ who investigated small-sized porous LAE442 cylinders with the same coatings in vitro in simulated body fluid, it was also revealed that the additional CaP coating increases the corrosion resistance of the cylinders.

The present study showed that 14/40 scaffolds (per group, $n=7$) exhibited increased degradation with loss of original shape compared to the remaining 26/40 scaffolds. It has been described in the literature that increased corrosion

in magnesium alloys can be caused by microstructural features, such as segregations of alloying elements or second phases that have higher electrode potential compared with the magnesium matrix.^{62–64} In the present study, SEM/EDS analyses detected local enrichments of the alloying elements rare earths and aluminum that increase the risk of microgalvanic corrosion. Furthermore, Denkena et al. reported⁶⁵ that the corrosion of bone substitute material depends significantly on stress, with compressive stress increasing the corrosion rate and tensile stresses reducing it. Due to the natural geometry of the rabbit tibia, asymmetric stress may affect the scaffold, resulting in different local corrosion rates. This might have been the case in the present study. Histologically, crack formation was noticed in the scaffold material, which was more severe in group 1 than in group 2, which might be related to the more severe degradation of MgF_2 scaffolds. Crack formation was also seen in other in vivo studies of implants or bone substitutes made of LAE442 or Mg alloys.^{27,60,61,66,67} According to Mueller et al.,⁶⁷ cracks occur in magnesium alloys due to gas evolution during degradation.

Furthermore, in the present study, there was radiographic evidence of proximal and distal osteotomy gaps between bone and the scaffold in the first few weeks post-op. It is possible that this was physiological bone necrosis of a few millimeters according to Muhr,⁶⁸ which generally occurs in the course of indirect fracture healing due to a lack of vascularization in the defect area. However, the visible gap could also be related to degradation and the resulting gas which displaced the callus network, creating the impression of reduced bone-scaffold contact. This needs to be clarified by further investigation.

The bone defect in the open wedge corrective osteotomy performed in this study healed via secondary bone healing, which was characterized by the formation of endosteal and periosteal callus tissue and was expected based on the size of the defect according to the literature.⁶⁹ A large amount of callus is considered positive in this type of bone healing, as it indicates a high healing capacity of the bone.^{70,71} According to the literature, the massive callus formation could also be due to the osteogenic potency of the magnesium ions.^{30,72,73} Initial callus formation could be found in all animals in the area of the lateral cortex (transcortex). One reason for increased lateral callus formation could have been the medially placed support plate. It can be assumed that this stabilization compensated part of the mechanical stress in the defect area of the medial rabbit tibia resulting in increased callus formation on the lateral side. This phenomenon was also found in other studies with plate-screw systems.^{13,74}

The transformation of callus/woven bone callus into lamellar bone over time seen in histology is known to occur in the course of secondary bone healing^{75–77} and was associated with a decrease in periosteal callus at later examination time points. Compared to periosteal callus formation, endosteal callus formation was observed to a

lesser extent and was also observed by Hampp et al.⁷⁸ investigating intramedullary pins of different magnesium alloys in rabbit tibiae.

In contrast to the study by Witting et al.²³ in this present study a larger scaffold and another implantation localization was used, which was in contact with surrounding soft tissue (in the case of cylinders purely cancellous position). According to the literature, Mg alloys degrade more rapidly when they are in contact with soft tissue, as at this location the blood flow is higher compared to cancellous bone.^{12,54,79,80} There was comparatively more loading on the scaffold due to the partial loaded defect and consequently a different degradation and bone ingrowth behavior of the scaffold compared to the cylinders. In the cylinders, there was more ingrowth of bone trabeculae, whereas in the wedge, the defect was primarily stabilized by callus and subsequently remodeled into lamellar bone.

When comparing the coatings, group 2 showed better bridging of the osteotomy gap and more bone-scaffold contacts by week 12. This observation could be due to the osteoconductive influence of the released calcium ions from the coating which was also observed in other *in vivo* studies.^{34,72} However, at later time points, better bridging, more bone scaffold contacts, and greater remodeling were seen in group 1 in our study. These could be explained by the overall greater degradation of the MgF₂ scaffolds at later time points. This stronger degradation might have released more magnesium ions which, according to the literature, have a high osteogenic potency.⁷³ From this it can be concluded that the influence of an additional CaP coating decreased over time.

Histologically, cartilaginous tissue was detected in some scaffolds (9/40) of both groups in the area of the scaffold tip, especially at the 6-week time point. This observation can be considered physiological, as the body attempts to close the defect via osteochondral ossification.^{76,81} Pauwels⁸² postulated that massive callus formation with predominantly osteochondral ossification predominates on the compression side of a weight-bearing fracture, which was presumably the case in the present study.

In the histological sections, a small amount of granulation tissue with fibroblasts was seen in both groups, although the percentage measured histomorphometrically was relatively constant over time in group 1 and varied slightly in group 2. According to the literature, the presence of granulation tissue can also be seen as a physiological response to a foreign body.⁸³ In the present study, granulation tissue and osteoid did not appear in the central pores until week 36. Mineralized bone tissue was not detected. Interconnecting pores in bone substitutes are thought to guide tissue growth, to enable and enhance tissue regeneration and blood flow, and to have an osteoconductive effect.^{64,84,85} According to the literature, pores in bone substitutes should have a size of 150–500 μm.^{86,87} The alloy LAE442 showed improved osteoconductive

properties in a previous study where 500 μm interconnecting pores were used, therefore this pore size was also chosen for the scaffolds in the present study.^{21,61}

The delayed ingrowth of bone tissue in the present study was also reported by Lalk et al.,²⁰ who found non mineralized bone tissue in the center of porous AX30 cylinders after 24 weeks. However, it must also be noted that the wedge used in the present study was much larger compared to the cylindrical implants, and thus the distance for ingrowing tissue into the scaffold center was much greater. Grau et al.⁸⁸ were also unable to see ingrowth of bone tissue into a porous magnesium implant in a skullcap defect in mice after 12 weeks. They hypothesized that the occupation of the implant center and pores with gas prevented bone ingrowth or delayed it. In both groups of the present study, bone marrow with adipocytes and hematopoietic cells were detected in the medullary canal at all time points which can be considered physiological.

The presence of some macrophages and only a few foreign body giant cells in the present study was related to scaffold degradation and removal of corrosion products, as also reported in the literature.^{17,19,61} These cells occur physiologically as part of a foreign body reaction in implanted biodegradable materials.^{60,89}

Blood vessels were detected in the histological examination at all times and their quantity increased over time. In week 36, more blood vessels were evident in group 1 compared to group 2. Improved vascularization results in better nutrient delivery, and thus better osseointegration.^{87,90–92} The better osseointegration of the more vascularized MgF₂ scaffolds compared to CaP scaffolds was also confirmed by higher bone quantities and more bone-scaffold contacts at later time points.

Furthermore, SEM images showed a dark degradation layer at the edge of the light-colored original scaffold material which increased with time. This observation is consistent with that of Kleer-Reiter et al.,⁶⁰ who studied porous cylindrical LAE442 scaffolds in the proximal rabbit femur. The fact that the proportion of Mg decreases as degradation progresses was also reported in *in vivo* studies with Mg-based implants by Wang et al.⁷² and Bracht et al.⁹³

On the surface and in the degradation layer of the scaffolds used in the present study, calcium- and phosphate-rich regions were measured in the EDS analyses. These calcium- and phosphate-rich regions provided direct contact between the scaffold and the surrounding bone tissue. In other studies with porous scaffolds of different magnesium alloys, these contacts were also seen^{30,60,61} and can be considered positive.

Conclusion

Wedge-shaped scaffolds of the magnesium alloy LAE442 showed good clinical tolerance, bridging of the osteotomy gap, and slow but inhomogeneous degradation with a single

MgF₂ coating (group 1) or an additional CaP coating (group 2). Increased bone-scaffold contacts were more pronounced until week 12 in group 2 (MgF₂-CaP coating), however at later timepoints in group 1 (MgF₂ coating). Therefore, a decreasing influence of CaP coating at later timepoints is assumed. However, CaP coating was shown to be beneficial for the first 12 weeks in the important phase of bone healing. The strong callus formation resulted in rapid stabilization of the defect in both groups. A population of undesired cells could not be found histologically. However, the production of these scaffolds in this shape and size was difficult.³⁷ The scaffolds already showed a certain inhomogeneity before implantation, which led to inhomogeneous degradation. Furthermore, despite the use of an additional CaP coating, the accumulation of gas could not be prevented.

Acknowledgements

The authors thank Beatrix Limmer, Cristiane Meneghelli-Rudolph, and Lisa Wurm for their excellent technical support, Yury Zablotzki for his help during the statistical analyses and Brigitte von Rechenberg for her assistance with the histological evaluation.

Contributorship

Conceptualization, H.J.M., P.W., and A.M.-L.; funding acquisition, H.J.M., P.W., and A.M.-L.; implementation of scaffold production S.J., C.K., and H.J.M.; gaining ethical approval, A.-C.W. and A.M.-L.; methodology and evaluation of in vivo and ex vivo investigations, M.S., F.F., A.-C.W., and A.M.-L.; project administration A.M.-L., P.W., and H.J.M.; supervision, F.F., A.-C.W., and A.M.-L.; visualization, M.S.; writing and original draft preparation, M.S.; all authors reviewed and edited the manuscript and approved the final version of the manuscript.

Data availability statement

The data of this study that substantiate the findings can be requested from the corresponding author upon request.

Declaration of conflicting interests

The author(s) declared no potential conflicts of interest with respect to the research, authorship, and/or publication of this article.

Funding

The author(s) disclosed receipt of the following financial support for the research, authorship, and/or publication of this article: This project was financially supported by the German Research Foundation (DFG) within the project “Interfacial effects and ingrowth behavior of magnesium sponges as a bioresorbable bone graft substitute” (Grant No. 271761343).

Guarantor

A.M.-L. takes full responsibility for this article, including the accuracy of the study as well as the appropriateness of the reference list.

ORCID iDs

Marlene Schmidt  <https://orcid.org/0000-0002-0030-5280>

Franziska Feichtner  <https://orcid.org/0000-0003-2435-1967>

Supplemental material

Supplemental material for this article is available online.

References

- Dimitriou R, Jones E, McGonagle D and Giannoudis PV. Bone regeneration: current concepts and future directions. *BMC Med* 2011; 9: 66–77.
- Parikh SN. Bone graft substitutes: past, present, future. *J Postgrad Med* 2002; 48: 142–148.
- Cipitria A, Reichert JC, Epari DR, et al. Polycaprolactone scaffold and reduced rhBMP-7 dose for the regeneration of critical-sized defects in sheep tibiae. *Biomaterials* 2013; 34: 9960–9968.
- Seiler J 3rd and Johnson J. Iliac crest autogenous bone grafting: donor site complications. *J South Orthop Assoc* 2000; 9: 91–97.
- Linhart W, Briem D, Amling M, Rueger JM and Windolf J. [Mechanical failure of porous hydroxyapatite ceramics 7.5 years after implantation in the proximal tibial]. *Unfallchirurg* 2004; 107: 154–157.
- Younger EM and Chapman MW. Morbidity at bone graft donor sites. *J Orthop Trauma* 1989; 3: 192–195.
- Salgado AJ, Coutinho OP and Reis RL. Bone tissue engineering: state of the art and future trends. *Macromol Biosci* 2004; 4: 743–765.
- Oryan A, Alidadi S, Moshiri A and Maffulli N. Bone regenerative medicine: classic options, novel strategies, and future directions. *J Orthop Surg Res* 2014; 9: 18.
- Gogolewski S. Bioresorbable polymers in trauma and bone surgery. *Injury* 2000; 31 Suppl 4: 28–32.
- Hofmann GO. Biodegradable implants in traumatology: a review on the state-of-the-art. *Arch Orthop Trauma Surg* 1995; 114: 123–132.
- Böstman O and Pihlajamäki H. Clinical biocompatibility of biodegradable orthopaedic implants for internal fixation: a review. *Biomaterials* 2000; 21: 2615–2621.
- Henderson SE, Verdelis K, Maiti S, et al. Magnesium alloys as a biomaterial for degradable craniofacial screws. *Acta Biomater* 2014; 10: 2323–2332.
- Tian L, Sheng Y, Huang L, et al. An innovative Mg/Ti hybrid fixation system developed for fracture fixation and healing enhancement at load-bearing skeletal site. *Biomaterials* 2018; 180: 173–183.
- Witte F. The history of biodegradable magnesium implants: a review. *Acta Biomater* 2010; 6: 1680–1692.
- Li X, Liu X, Wu S, Yeung KWK, Zheng Y and Chu PK. Design of magnesium alloys with controllable degradation for biomedical implants: from bulk to surface. *Acta Biomater* 2016; 45: 2–30.
- Rössig C, Angrisani N, Besdo S, et al. Magnesium-based intramedullary nailing system in a sheep model: biomechanical evaluation and first in vivo results. *J Vet Sci Med Diagn* 2014; 4: 1–12.
- Angrisani N, Reifenrath J, Zimmermann F, et al. Biocompatibility and degradation of LAE442-based

- magnesium alloys after implantation of up to 3.5 years in a rabbit model. *Acta Biomater* 2016; 44: 355–365.
18. Windhagen H, Radtke K, Weizbauer A, et al. Biodegradable magnesium-based screw clinically equivalent to titanium screw in hallux valgus surgery: short term results of the first prospective, randomized, controlled clinical pilot study. *Biomed Eng Online* 2013; 12: 62.
 19. Lalk M, Reifenrath J, Angrisani N, et al. Fluoride and calcium-phosphate coated sponges of the magnesium alloy AX30 as bone grafts: a comparative study in rabbits. *J Mater Sci Mater Med* 2013; 24: 417–436.
 20. Lalk M, Reifenrath J, Rittershaus D, Bormann D and Meyer-Lindenberg A. Biocompatibility and degradation behaviour of degradable magnesium sponges coated with bioglass - method establishment within the framework of a pilot study. *Materwiss Werksttech* 2010; 41: 1025–1034.
 21. Augustin J, Feichtner F, Waselau A, et al. Comparison of two pore sizes of LAE442 scaffolds and their effect on degradation and osseointegration behavior in the rabbit model. *J Biomed Mater Res A* 2020; 108: 2776–2788.
 22. Kleer N, Julmi S, Gartzke A-K, et al. Comparison of degradation behaviour and osseointegration of the two magnesium scaffolds, LAE442 and La2, in vivo. *Materialia* 2019; 8: 100436.
 23. Witting LM, Waselau A-C, Feichtner F, et al. Influence of coatings on degradation and osseointegration of open porous Mg scaffolds in vivo. *Materialia* 2020; 14: 100949.
 24. Zhang Y, Xu J, Ruan YC, et al. Implant-derived magnesium induces local neuronal production of CGRP to improve bone-fracture healing in rats. *Nat Med* 2016; 22: 1160–1169.
 25. Chaya A, Yoshizawa S, Verdelis K, et al. In vivo study of magnesium plate and screw degradation and bone fracture healing. *Acta Biomater* 2015; 18: 262–269.
 26. Revell PA, Damien E, Zhang XS, Evans P and Howlett CR. The effect of magnesium ions on bone bonding to hydroxyapatite coating on titanium alloy implants. *Key Eng Mater* 2004; 254–256: 447–450.
 27. Thomann M, Krause C, Angrisani N, et al. Influence of a magnesium-fluoride coating of magnesium-based implants (MgCa0.8) on degradation in a rabbit model. *J Biomed Mater Res A* 2010; 93: 1609–1619.
 28. Shao Y, Zeng R-C, Li SQ, et al. Advance in antibacterial magnesium alloys and surface coatings on magnesium alloys: a review. *Acta Metallurgica Sin* 2020; 33: 615–629.
 29. Smith MR, Atkinson P, White D, et al. Design and assessment of a wrapped cylindrical Ca-P AZ31 Mg alloy for critical-size ulna defect repair. *J Biomed Mater Res A* 2012; 100B: 206–216.
 30. Witte F, Kaese V, Haferkamp H, et al. In vivo corrosion of four magnesium alloys and the associated bone response. *Biomaterials* 2005; 26: 3557–3563.
 31. Kopp A, Derra T, Mütter M, et al. Influence of design and postprocessing parameters on the degradation behavior and mechanical properties of additively manufactured magnesium scaffolds. *Acta Biomater* 2019; 98: 23–35.
 32. Alvarez-Lopez M, Pereda MD, del Valle JA, et al. Corrosion behaviour of AZ31 magnesium alloy with different grain sizes in simulated biological fluids. *Acta Biomater* 2010; 6: 1763–1771.
 33. Staiger MP, Pietak AM, Huadmai J and Dias G. Magnesium and its alloys as orthopedic biomaterials: a review. *Biomaterials* 2006; 27: 1728–1734.
 34. Thomann M, Krause C, Bormann D, von der Höh N, Windhagen H and Meyer-Lindenberg A. Comparison of the resorbable magnesium alloys LAE442 und MgCa0.8 concerning their mechanical properties, their progress of degradation and the bone-implant-contact after 12 months implantation duration in a rabbit model. *Materwiss Werksttech* 2009; 40: 82–87.
 35. Reifenrath J, Krause A, Bormann D, von Rechenberg B, Windhagen H and Meyer-Lindenberg A. Profound differences in the in-vivo-degradation and biocompatibility of two very similar rare-earth containing Mg-alloys in a rabbit model. *Materwiss Werksttech* 2010; 41: 1054–1061.
 36. Maier HJ, Julmi S, Behrens S, et al. Magnesium alloys for open-pored bioresorbable implants. *JOM* 2020; 72: 1859–1869.
 37. Julmi S, Krüger A-K, Waselau A-C, et al. Processing and coating of open-pored absorbable magnesium-based bone implants. *Mater Sci Eng C* 2019; 98: 1073–1086.
 38. Song G. Control of biodegradation of biocompatible magnesium alloys. *Corros Sci* 2007; 49: 1696–1701.
 39. Witte F, Fischer J, Nellesen J, et al. In vivo corrosion and corrosion protection of magnesium alloy LAE442. *Acta Biomater* 2010; 6: 1792–1799.
 40. Staesche M. Über die chemische Erzeugung einer dickeren magnesiumfluorid-schutzschicht auf magnesium-legierungen. *Arch für Metallkunde* 1948; 3: 99–102.
 41. Jo JH, Kang B-G, Shin K-S, et al. Hydroxyapatite coating on magnesium with MgF- interlayer for enhanced corrosion resistance and biocompatibility. *J Mater Sci Mater Med* 2011; 22: 2437–2447.
 42. da Silva D, Kaduri M, Poley M, et al. Biocompatibility, biodegradation and excretion of polylactic acid (PLA) in medical implants and theranostic systems. *Chem Eng J* 2018; 340: 9–14.
 43. Tanodekaew S, Channasanon S, Kaewkong P and Uppanan P. PLA-HA scaffolds: preparation and bioactivity. *Procedia Eng* 2013; 59: 144–149.
 44. Song Y, Zhang S, Li J, Zhao C and Zhang X. Electrodeposition of Ca-P coatings on biodegradable Mg alloy: in vitro biomineralization behavior. *Acta Biomater* 2010; 6: 1736–1742.
 45. Waterman J, Birbilis N, Dias GJ, Woodfield TBF and Staiger MP. Improving *in vitro* corrosion resistance of biomimetic calcium phosphate coatings for Mg substrates using calcium hydroxide layer. *Corros Eng Sci Technol* 2012; 47: 340–345.
 46. Waterman J, Pietak A, Birbilis N, Woodfield T, Dias G and Staiger MP. Corrosion resistance of biomimetic calcium phosphate coatings on magnesium due to varying pretreatment time. *Mater Sci Eng B* 2011; 176: 1756–1760.
 47. Julmi S, Klose C, Krüger A-K, et al. Development of sponge structure and casting conditions for absorbable magnesium bone implants. In: *TMS 2017 146th annual meeting & exhibition supplemental proceedings*, 2017, pp.307–317. Cham: Springer.
 48. Seitz JM, Collier K, Wulf E, Bormann D and Bach FW. Comparison of the corrosion behavior of coated and

- uncoated magnesium alloys in an in vitro corrosion environment. *Adv Eng Mater* 2011; 13: B313–B323.
49. Spoor CF, Zonneveld FW and Macho GA. Linear measurements of cortical bone and dental enamel by computed tomography: applications and problems. *Am J Phys Anthropol* 1993; 91: 469–484.
 50. Donath K and Breuner G. A method for the study of undecalcified bones and teeth with attached soft tissues. The Sage-Schliff (sawing and grinding) technique. *J Oral Pathol Med* 1982; 11: 318–326.
 51. Witte F, Fischer J, Nellesen J, et al. In vitro and in vivo corrosion measurements of magnesium alloys. *Biomaterials* 2006; 27: 1013–1018.
 52. Wu Y, Wang YM, Zhao DW, et al. In vivo study of micro-arc oxidation coated Mg alloy as a substitute for bone defect repairing: degradation behavior, mechanical properties, and bone response. *Colloids Surf B Biointerfaces* 2019; 181: 349–359.
 53. Witte F, Hort N, Vogt C, et al. Degradable biomaterials based on magnesium corrosion. *Curr Opin Solid State Mater Sci* 2008; 12: 63–72.
 54. Zhang N, Zhao D, Liu N, et al. Assessment of the degradation rates and effectiveness of different coated Mg-Zn-Ca alloy scaffolds for in vivo repair of critical-size bone defects. *J Mater Sci Mater Med* 2018; 29: 138.
 55. Erdmann N, Bondarenko A, Hewicker-Trautwein M, et al. Evaluation of the soft tissue biocompatibility of MgCa0.8 and surgical steel 316L in vivo: a comparative study in rabbits. *Biomed Eng Online* 2010; 9: 63.
 56. Bondarenko A, Angrisani N, Meyer-Lindenberg A, Seitz JM, Waizy H and Reifenrath J. Magnesium-based bone implants: immunohistochemical analysis of peri-implant osteogenesis by evaluation of osteopontin and osteocalcin expression. *J Biomed Mater Res A* 2013; 102: 1449–1457.
 57. Rössig C, Angrisani N, Helmecke P, et al. In vivo evaluation of a magnesium-based degradable intramedullary nailing system in a sheep model. *Acta Biomater* 2015; 25: 369–383.
 58. Baroudi R and Ferreira CA. Seroma: how to avoid it and how to treat it. *Aesthet Surg J* 1998; 18: 439–441.
 59. Garrett MP, Kakarla UK, Porter RW and Sonntag VK. Formation of painful seroma and edema after the use of recombinant human bone morphogenetic protein-2 in posterolateral lumbar spine fusions. *Neurosurg* 2010; 66: 1044–1049.
 60. Kleer-Reiter N, Julmi S, Feichtner F, et al. Biocompatibility and degradation of the open-pored magnesium scaffolds LAE442 and La2. *Biomed Mater* 2021; 16: 035037.
 61. Augustin J, Feichtner F, Waselau A-C, et al. Effect of pore size on tissue ingrowth and osteoconductivity in biodegradable Mg alloy scaffolds. *J Appl Biomater Funct Mater* 2022; 20: 22808000221078168.
 62. Huehnerschulte TA, Angrisani N, Rittershaus D, Bormann D, Windhagen H and Meyer-Lindenberg A. In vivo corrosion of two novel magnesium alloys ZEK100 and AX30 and their mechanical suitability as biodegradable implants. *Materials* 2011; 4: 1144–1167.
 63. Song GL and Atrens A. Corrosion mechanisms of magnesium alloys. *Adv Eng Mater* 1999; 1: 11–33.
 64. Gartzke A-K, Julmi S, Klose C, et al. A simulation model for the degradation of magnesium-based bone implants. *J Mech Behav Biomed Mater* 2020; 101: 103411.
 65. Denkena B, Köhler J, Stieghorst J, et al. Influence of stress on the degradation behavior of Mg LAE442 implant systems. *Procedia CIRP* 2013; 5: 189–195.
 66. Ullmann B, Reifenrath J, Seitz J-M, Bormann D and Meyer-Lindenberg A. Influence of the grain size on the in vivo degradation behaviour of the magnesium alloy LAE442. *Proc IMechE, Part H: J Engineering in Medicine* 2013; 227: 317–326.
 67. Mueller W-D, de Mele MF, Nascimento ML and Zeddies M. Degradation of magnesium and its alloys: dependence on the composition of the synthetic biological media. *J Biomed Mater Res A* 2009; 90: 487–495.
 68. Muhr G. Die bedeutung von biologie und biomechanik in der frakturheilung. In: Oestern HJ and Probst J (eds) *Unfallchirurgie in deutschland*. Berlin, Heidelberg: Springer, 1997, pp.128–134.
 69. Stürmer K. Histomorphologie der frakturheilung im vergleich der fixationsverfahren am tibiaschaft. In: Schmit-Neuerburg KP and Stürmer KM (eds) *Die tibiaschaftfraktur beim erwachsenen*. Berlin, Heidelberg: Springer, 1987, pp.23–49.
 70. Einhorn TA and Gerstenfeld LC. Fracture healing: mechanisms and interventions. *Nat Rev Rheumatol* 2015; 11: 45–54.
 71. Féron J-M and Mauprivez R. Fracture repair: general aspects and influence of osteoporosis and anti-osteoporosis treatment. *Injury* 2016; 47: 10–14.
 72. Wang W, Nune KC, Tan L, et al. Bone regeneration of hollow tubular magnesium-strontium scaffolds in critical-size segmental defects: effect of surface coatings. *Mater Sci Eng C* 2019; 100: 297–307.
 73. Janning C, Willbold E, Vogt C, et al. Magnesium hydroxide temporarily enhancing osteoblast activity and decreasing the osteoclast number in peri-implant bone remodelling. *Acta Biomater* 2010; 6: 1861–1868.
 74. Wieding J, Lindner T, Bergschmidt P and Bader R. Biomechanical stability of novel mechanically adapted open-porous titanium scaffolds in metatarsal bone defects of sheep. *Biomaterials* 2015; 46: 35–47.
 75. Schindeler A, McDonald MM, Bokko P and Little DG. Bone remodeling during fracture repair: the cellular picture. *Semin Cell Dev Biol* 2008; 19: 459–466.
 76. Lanske B, Chandler H, Pierce A, et al. Abaloparatide, a PTH receptor agonist with homology to PTHrP, enhances callus bridging and biomechanical properties in rats with femoral fracture. *J Orthop Res* 2019; 37: 812–820.
 77. Herten M, Zilkens C, Thorey F, et al. Biomechanical stability and osteogenesis in a tibial bone defect treated by autologous ovine cord blood cells—a pilot study. *Molecules* 2019; 24: 295.
 78. Hampp C, Angrisani N, Reifenrath J, Bormann D, Seitz JM and Meyer-Lindenberg A. Evaluation of the biocompatibility of two magnesium alloys as degradable implant materials in comparison to titanium as non-resorbable material in the rabbit. *Mater Sci Eng C* 2013; 33: 317–326.
 79. Wolters L, Angrisani N, Seitz J, Helmecke P, Weizbauer A and Reifenrath J. Applicability of degradable magnesium

- LAE442 alloy plate-screw-systems in a rabbit model. *Biomed Eng* 2013; 58. DOI: 10.1515/bmt-2013-4059
80. Simon SR. *Orthopaedic basic science*. Rosemont, IL: Amer Academy of Orthopaedic, 1994.
 81. Ford JL, Robinson DE and Scammell BE. The fate of soft callus chondrocytes during long bone fracture repair. *J Orthop Res* 2003; 21: 54–61.
 82. Pauwels F. Eine neue Theorie über den Einfluß mechanischer Reize auf die Differenzierung der Stützgewebe. *Z Anat Entwicklungsgesch* 1960; 121: 478–515.
 83. Gu XN, Xie XH, Li N, Zheng YF and Qin L. In vitro and in vivo studies on a Mg-Sr binary alloy system developed as a new kind of biodegradable metal. *Acta Biomater* 2012; 8: 2360–2374.
 84. Song J, Kim J, Woo H-M, et al. Repair of rabbit radial bone defects using bone morphogenetic protein-2 combined with 3D porous silk fibroin/ β -tricalcium phosphate hybrid scaffolds. *J Biomater Sci Polym Ed* 2018; 29: 716–729.
 85. Cipitria A, Lange C, Schell H, et al. Porous scaffold architecture guides tissue formation. *J Bone Miner Res* 2012; 27: 1275–1288.
 86. Klenke FM, Liu Y, Yuan H, Hunziker EB, Siebenrock KA and Hofstetter W. Impact of pore size on the vascularization and osseointegration of ceramic bone substitutes in vivo. *J Biomed Mater Res A* 2008; 85: 777–786.
 87. Karageorgiou V and Kaplan D. Porosity of 3D biomaterial scaffolds and osteogenesis. *Biomaterials* 2005; 26: 5474–5491.
 88. Grau M, Seiler C, Roland L, et al. Osteointegration of porous poly- ϵ -caprolactone-coated and previtalised magnesium implants in critically sized calvarial bone defects in the mouse model. *Materials* 2018; 11: 6.
 89. Nuss KM and von Rechenberg B. Biocompatibility issues with modern implants in bone - a review for clinical orthopedics. *Open Orthop J* 2008; 2: 66–78.
 90. Cheng MQ, Wahafu T, Jiang GF, et al. A novel open-porous magnesium scaffold with controllable microstructures and properties for bone regeneration. *Sci Rep* 2016; 6: 24134.
 91. Pawelec K and Planell JA. *Bone repair biomaterials: regeneration and clinical applications*. Duxford: Woodhead Publishing, 2019.
 92. Mavrogenis AF, Dimitriou R, Parvizi J and Babis GC. Biology of implant osseointegration. *J Musculoskelet Neuronal Interact* 2009; 9: 61–71.
 93. Bracht K, Angrisani N, Seitz J-M, Eifler R, Weizbauer A and Reifenrath J. The influence of storage and heat treatment on a magnesium-based implant material: an in vitro and in vivo study. *Biomed Eng Online* 2015; 14: 1–17.